Four-Wave Mixing Signal Shaping Scheme Using Semiconductor Optical Amplifier for Optical Communication Systems

S. R. Hosseini[1, 2*], M. Razaghi[1], *Member, IEEE,* and N. K. Das[3], *Senior Member, IEEE*

***Abstract*—We have numerically analysed the effects of SOA's medium length on four-wave mixing (FWM) characteristics in semiconductor optical amplifier (SOA). We have studied the shape, spectrum, full width at half maximum (FWHM), time-bandwidth product, peak shift and frequency shift of the FWM signal for weak and strong input pump and probe pulses. We have used the nonlinear propagation equation taking into account gain spectrum dynamic gain saturation which depends on carrier depletion, carrier heating, spectral hole-burning, group velocity dispersion, self phase modulation and two photon absorption. We have used finite-difference beam propagation method (FD-BPM) to simulate the wave evolution both in time and spectral domain in the SOA. From this simulation, it has become clear that the FWM signal characteristics are dependent to the length of SOA. In high power regime, nonlinear phenomena in SOA have more influences on the FWM signal characteristics.**

***Index Terms*—Semiconductor optical amplifier, SOA length, pulse shape, spectrum, FWHM, band width, time-width product, peak shift, spectral shift.**

I. Introduction

Recently, semiconductor optical amplifiers (SOAs) have significant practical interest in data communication applications, because of their small size, high optical gain, low input power requirement, faster response time, large bandwidth and compatible optoelectronic characteristics [1-4]. SOAs are useful to amplify the short pulses and to contribute in ultrahigh-speed optical communication systems. Nonlinear effects are the basis of many schemes in ultrahigh-speed optical communication systems and devices, such as, all-optical modulators, demultiplexers and 3R regenerators that require very fast dynamics in a fibre and in semiconductor devices. SOA is one of the fundamental parts of the large-scale integration and nonlinear effects play an important role in pulse shaping process in it [3-4].

The main objective of this paper is to investigate how the length of the propagation medium affects the shape, spectrum, full width at half maximum (FWHM), time-bandwidth product and peak shift of the FWM signal in the SOA. To attain our goal, we have numerically simulated theoptical wave propagation in the SOA. The beam propagation method (BPM) is widely used for the analysis of the field distribution in optical waveguides and optical pulse propagation in fibers [5]. Usually, this is the best method for simulating optical pulse propagation with small propagation steps and has the potential for wide application. Based on the simulation time and results, we used the FD-BPM, because of short convergence time and excellent accuracy of the results [3-6]. All the characteristics of the FWM pulse have studied for weak and strong input pump and probe pulse energies.

This paper is organized as follow; Section 1 is Introduction, Section 2 is Analytical Model, the equations which govern the dynamics of the amplification process, Section 3 is Simulation Results and Discussion and finally Conclusions are in Section 4.

II. Analytical Model

A. Pulse propagation

The model we have used is based on modified nonlinear Schrödinger equation which explains the propagation of optical pulse in the SOA's medium [7].

$$\left[\frac{\partial}{\partial z}-\frac{i}{2}\beta_2\frac{\partial^2}{\partial\tau^2}+\frac{\gamma}{2}+\left(\frac{\gamma_{2p}}{2}+ib_2\right)\left|V(z,\tau)\right|^2\right]V(z,\tau)$$
$$=\left\{\frac{1}{2}g_N(\tau)\left[\frac{1}{f_T(\tau)}+i\alpha_N\right]+\frac{1}{2}\Delta g_T(\tau)\left(1+i\alpha_T\right)\right.$$
$$\left.-i\frac{1}{2}\frac{\partial g(\tau,\omega)}{\partial\omega}\bigg|_{\omega_0}\frac{\partial}{\partial\tau}-\frac{1}{4}\frac{\partial^2 g(\tau,\omega)}{\partial\omega^2}\bigg|_{\omega_0}\frac{\partial^2}{\partial\tau^2}\right\}V(z,\tau) \quad (1)$$

where, $V(z,\tau)$ is the complex envelope function of an optical pulse. The definitions of some parameters in the equation are as follow:

$$g_N(\tau)=g_0\exp\left(-\frac{1}{E_{sat}}\int_{-\infty}^{\tau}e^{-s/\tau_s}\left|V(s)\right|^2ds\right) \quad (2)$$

$$f(\tau)=1+\frac{1}{\tau_{shb}P_{shb}}\int_{-\infty}^{+\infty}u(s)e^{-s/\tau_{shb}}\left|V(\tau-s)\right|^2ds \quad (3)$$

$$\Delta g_T(\tau)=-h_1\int_{-\infty}^{+\infty}u(s)e^{-s/\tau_{ch}}\times(1-e^{-s/\tau_{shb}})\left|V(\tau-s)\right|^2ds$$
$$-h_2\int_{-\infty}^{+\infty}u(s)e^{-s/\tau_{ch}}\times(1-e^{-s/\tau_{shb}})\left|V(\tau-s)\right|^4ds \quad (4)$$

[1]Dept. of Electrical and Computer Engineering, University of Kurdistan, Sanandaj, Iran, P.O. Box 416.
[2]Dept. of Physics, University of Kurdistan, Sanandaj, Iran, P.O. Box 416.
[3]Electron Science Research Institute, Edith Cowan University, Joondalup, WA, 6027, Australia.
[*]Corresponding author phone: Tel.: +98 871 6624774; fax: +98 871 6660073; e-mail: rasoul.hosseini@uok.ac.ir

$$\left.\frac{\partial g(\tau,\omega)}{\partial \omega}\right|_{\omega_0} = A_1 + B_1\left[g_0 - g(\tau,\omega_0)\right] \tag{5}$$

$$\left.\frac{\partial^2 g(\tau,\omega)}{\partial \omega^2}\right|_{\omega_0} = A_2 + B_2\left[g_0 - g(\tau,\omega_0)\right] \tag{6}$$

$$g(\tau,\omega_0) = g_N(\tau,\omega_0)/f(\tau) + \Delta g_T(\tau,\omega_0) \tag{7}$$

where, $\tau = t - z/v_g$ is the frame of local time which propagates with the group velocity v_g of the optical pulse at central frequency. The slowly varying envelope function approximation is used in Eq. (1), where the temporal variation change of the complex envelope function is very slow compared with the cycle of an optical field. $|V(z,\tau)|^2$ is the optical power (intensity), β_2 is the group velocity dispersion (GVD), γ is linear loss, γ_{2p} is the two-photon absorption coefficient, $b_2(=\omega_0 n_2/cA)$ is the instantaneous self-phase modulation term due to the Kerr effect, n_2 is an instantaneous nonlinear refractive index, $\omega_0(=2\pi f_0)$ is the center angular frequency of the pulse, c is the velocity of light in vacuum, $A(=wd/\Gamma)$ is the effective area (d and w are the thickness and width of the active region, respectively, and Γ is the confinement factor). $g_N(\tau)$ is the saturated gain due to carrier depletion, g_0 is the linear gain, E_{sat} is the saturation energy, τ_s is the carrier lifetime, $f(\tau)$ is the spectral hole-burning function, P_{shb} is the spectral hole-burning saturation power, τ_{shb} is the spectral hole-burning relaxation time, and α_N and α_T are the linewidth enhancement factor associated with the gain changes due to the carrier depletion and carrier heating. $\Delta g_T(\tau)$ is the resulting gain change due to the carrier heating and two-photon absorption, $u(s)$ is the unit step function, τ_{ch} is the carrier heating relaxation time, h_1 is the contribution of stimulated emission and free-carrier absorption to the carrier heating gain reduction, and h_2 is the contribution of two-photon absorption. Finally, A_1 and A_2 are the slope and the curvature of the linear gain at ω_0, respectively, while B_1 and B_2 are constants describing changes in these quantities with saturation [7-8].

This model includes the dynamic gain change terms, i.e. the first- and second-order gain spectrum terms which are the last two terms of the right side in (1), we cannot separate the linear propagation term (GVD term) and phase compensation terms (other than GVD, first- and second-order gain spectrum terms). Therefore, it is not possible to use the common methods like fast Fourier transformation BPM (FFT-BPM). Hence, we have used the finite difference beam propagation method (FD-BPM) [9]. If we replace the time derivative terms of (1) by the central-difference approximation (9) and integrate (1) with the small propagation step Δz, we obtain the tridiagonal simultaneous matrix (10),

$$\frac{\partial}{\partial \tau} V_k = \frac{V_{k+1} - V_{k-1}}{2\Delta\tau} \tag{8}$$

$$\frac{\partial^2}{\partial \tau^2} V_k = \frac{V_{k+1} - 2V_k + V_{k-1}}{\Delta\tau^2} \tag{9}$$

where, $V_k = V(\tau_k)$, $V_{k+1} = V(\tau_k + \Delta\tau)$, and $V_{k-1} = V(\tau_k - \Delta\tau)$

$$\begin{aligned} &-a_k(z+\Delta z)V_{k-1}(z+\Delta z) + \{1 - b_k(z+\Delta z)\} \\ &\quad \times V_k(z+\Delta z) - c_k(z+\Delta z)V_{k+1}(z+\Delta z) \\ &= a_k(z)V_{k-1}(z) + \{1 + b_k(z)\}V_k(z) + c_k(z)V_{k+1}(z) \end{aligned} \tag{10}$$

where $k = 1, 2, 3, ..., n$ and

$$\begin{aligned} a_k(z) = \frac{\Delta z}{2}\Bigg[&\frac{i\beta_2}{2\Delta\tau^2} + i\frac{1}{4\Delta\tau}\left.\frac{\partial g(\tau,\omega,z)}{\partial\omega}\right|_{\omega_0,\tau_k} \\ &- \frac{1}{4\Delta\tau^2}\left.\frac{\partial^2 g(\tau,\omega,z)}{\partial\omega^2}\right|_{\omega_0,\tau_k}\Bigg] \end{aligned} \tag{11}$$

$$\begin{aligned} b_k(z) = -\frac{\Delta z}{2}\Bigg[&\frac{i\beta_2}{\Delta\tau^2} + \frac{\gamma}{2} + \left(\frac{\gamma_{2p}}{2} + ib_2\right)|V_k(z)|^2 \\ &- \frac{1}{2}g_N(\tau_k,\omega_0,z)(1 + i\alpha_N) \\ &- \frac{1}{2}g_N(\tau_k,\omega_0,z)(1 + i\alpha_T) \\ &- \frac{1}{2\Delta\tau^2}\left.\frac{\partial^2 g(\tau,\omega,z)}{\partial\omega^2}\right|_{\omega_0,\tau_k}\Bigg] \end{aligned} \tag{12}$$

$$\begin{aligned} c_k(z) = \frac{\Delta z}{2}\Bigg[&\frac{i\beta_2}{2\Delta\tau^2} - i\frac{1}{4\Delta\tau}\left.\frac{\partial g(\tau,\omega,z)}{\partial\omega}\right|_{\omega_0,\tau_k} \\ &- \frac{1}{4\Delta\tau^2}\left.\frac{\partial^2 g(\tau,\omega,z)}{\partial\omega^2}\right|_{\omega_0,\tau_k}\Bigg] \end{aligned} \tag{13}$$

where, $\Delta\tau$ is the sampling time and n is the number of sampling. If we know $V_k(z)$, $(k = 1, 2, 3, ..., n)$ at position z, we can calculate $V_k(z+\Delta z)$ at position $z+\Delta z$ which is the propagation of a step Δz from position z, by using (10).

It is not possible to directly calculate (10) because it is necessary to calculate the left-side terms $a_k(z+\Delta z)$, $b_k(z+\Delta z)$ and $c_k(z+\Delta z)$ of (10) from the unknown $V_k(z+\Delta z)$. Therefore, we have initially defined $a_k(z+\Delta z) \equiv a_k(z)$, $b_k(z+\Delta z) \equiv b_k(z)$ and $c_k(z+\Delta z) \equiv c_k(z)$, and obtained $V_k^{(0)}(z+\Delta z)$, as the zeroeth order approximation of $V_k(z+\Delta z)$ by using (10). Then, we have substituted $V_k^{(0)}(z+\Delta z)$ in (10) and obtained $V_k^{(1)}(z+\Delta z)$ as the first-order approximation of $V_k(z+\Delta z)$ and finally obtained accurate simulation results by iteration [7].

B. Four-wave mixing (FWM)

When two optical pulses with different central frequencies of f_p (pump) and f_q (probe) are injected into the SOA simultaneously, the FWM signal is generated in the SOA at a frequency of $2f_p - f_q$. For the analysis of the nondegenerate FWM characteristics, we have used the

following equation for describing the two input pulses (pump and probe pulses), which are simultaneously injected into the SOA [7].

$$V(\tau) = V_p(\tau) + V_q(\tau)\exp(-i\Delta\omega\tau) \quad (14)$$

where, $V_p(\tau)$ and $V_q(\tau)$ are the complex envelope functions of the input pump and probe pulses, and $\Delta\omega$ is a detuning angular frequency expressed as $\Delta\omega = 2\pi f = 2\pi(f_p - f_q)$. Using the complex envelope function of (14), we get the solution of (1) and obtain the propagation characteristics of two pulses (amplified pump and probe) and the generated FWM signal in an SOA.

III. Results and Discussion

We have used the parameters of a bulk SOA (AlGaAs/GaAs, double heterostructure) with a wavelength of 0.86 μm in our simulation. The parameters are listed in Table I [7].

TABLE I
LIST OF PARAMETERS USED IN SIMULATION [7].

Symbol	Quantity	Value
L	SOA length	500 μm
A_r	Effective area	5 μm^2
f_0	Center frequency of the pulse	349 THz
β_2	Group velocity dispersion	0.05 ps^2cm^{-1}
E_{sat}	Saturation energy	80 PJ
α_N	Linewidth enhancement factor due to the carrier depletion	3.1
α_T	Linewidth enhancement factor due to the carrier heating	2.0
h_1	Contribution of stimulated emission and free carrier absorption to the carrier heating gain reduction	0.13 cm^{-1} pJ^{-1}
h_2	Contribution of stimulated emission and free carrier absorption to the carrier heating gain reduction	126 fs cm^{-1} pJ^{-1}
τ_s	Carrier lifetime	200 ps
τ_{ch}	Carrier heating relaxation time	700 ps
τ_{shb}	Spectral hole burning relaxation time	60 ps
τ_{shb}	Spectral hole burning relaxation power	28.3 W
γ	Linear loss	11.5 cm^{-1}
γ_{2p}	Two photon absorption coefficient	1.1 $cm^{-1}W^{-1}$
A_1		0.15 fs μm^{-1}
A_2	Parameters describing the second order	-80 fs
B_1	Taylor expansion of the dynamical gain	-60 $fs^2\mu m^{-1}$
B_2	spectrum	0 fs^2

The following results are achieved, when the input pulses are $sech^2$ shape and they are Fourier transform limited. The simulation results are verified by comparison with previously published results [3-4]. We have studied the FWM characteristics for weak and strong SOA input pulses (pump and probe). The energy of the weak input pump and probe pulses are $10\,fJ$ and $1\,fJ$ respectively and the energy of the strong input pump and probe pulses are $2\,pJ$ and $200\,fJ$ respectively.

A. FWM Signal Shape

Fig. 1(a) and Fig. 1(b) show the generated FWM signal shapes for weak and strong input pulses and for different SOA lengths, respectively.

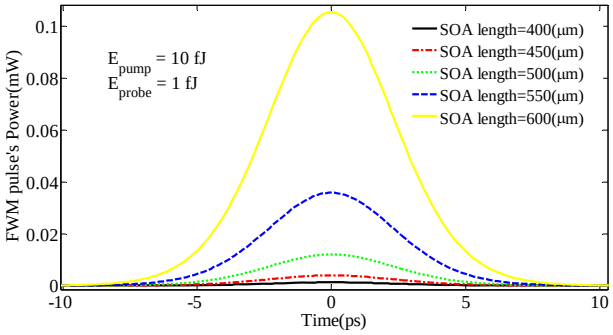

Fig. 1(a). The generated FWM signal shapes for various SOA lengths, for this case, the input pump and probe pulse energies are $10\,fJ$ and $1\,fJ$ respectively.

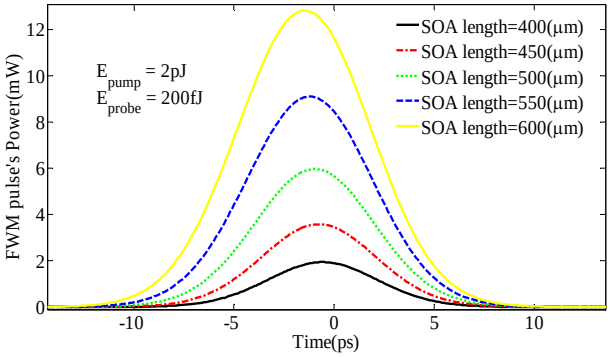

Fig. 1(b). The generated FWM signal shapes for various SOA lengths, for this case, the input pump and probe pulses energies are $2\,pJ$ and $200\,fJ$ respectively.

It has clearly shown that the power (energy) of the FWM pulse increases when the SOA length increases. $G_0 = \exp(g_0 L)$ is the unsaturated gain of the SOA and it has exponential relation to the length of the SOA. So, with increasing the SOA length leads to more amplified output pulse energy. Power (energy) increasing rate for weak input pulses are more in comparison to the strong input pulses. It is because the intensity of the FWM Pulse is related to $I_P{}^2 I_q$ where I_P is the pump pulse intensity and I_q is the probe pulse intensity [7].

B. FWM Signal Spectrum

Fig. 2(a) and Fig. 3(a) show the output spectrum of the SOA for weak and strong input pulses respectively. Pump pulse, probe pulse and generated FWM signal spectra have specified in figures. To be more visible, FWM signal spectra are illustrated in Fig. 2(b) and Fig. 3(b) for weak and strong input pulses, respectively.

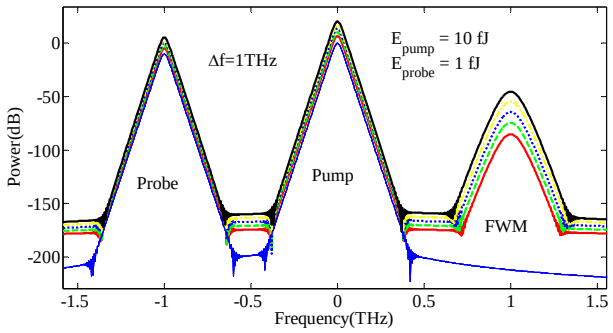

Fig. 2(a) Output pulse spectrum corresponding to the pulse shapes shown in Fig. 1(a).

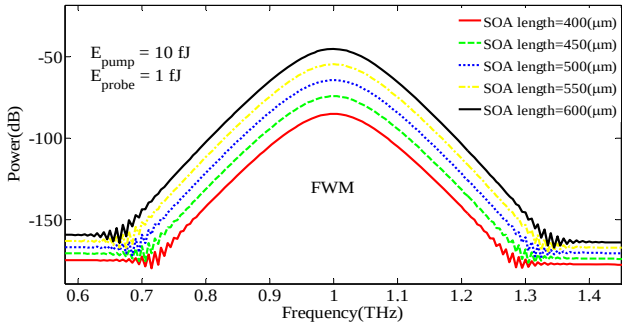

Fig. 2(b) The generated FWM signal spectrum for various SOA lengths, for this case, the input pump and probe pulse energies are $10\,fJ$ and $1\,fJ$ respectively.

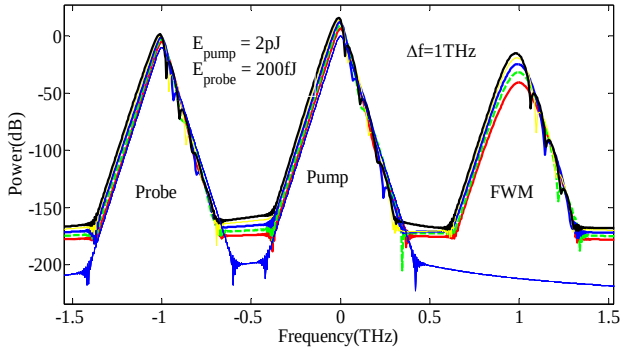

Fig. 3(a) Output pulse spectrum corresponding to the pulse shapes shown in Fig. 1(b)

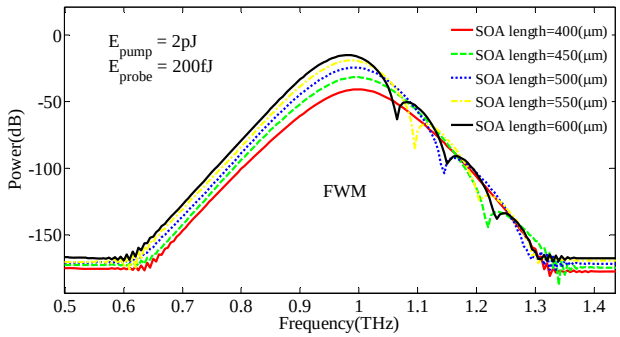

Fig. 3(b) The generated FWM signal spectrum for various values of SOA length, for this case, the input pump and probe pulse energies are $2\,pJ$ and $200\,fJ$ respectively.

As it has shown in Fig. 2(b), the spectrum of the FWM sinal is strongly dependent to the SOA length. For weak input pulses, there is no oscillation in the FWM pulse's spectrum. It is because the SOA is not saturated and as a result carrier depletion is not so effective.

Fig. 3(b) shows that for 400μm SOA, although the SOA input pulses are strong, the spectrum has not oscillatory structure. But, for 450μm and longer SOAs, the FWM spectrum experiences oscillation for the strong input pulses. The origin of these oscillatory structures comes from variation of carriers due to strong input pulses and instantaneous instructive or constructive interferences of optical waves in the wave guide [5]. When the input pump and probe pulses are strong, the SOA will saturate and the nonlinear phenomena will emerge. Moreover, when the SOA length increases, optical waves have more time to propagate in the SOA medium and as a result, more time to interfere. So, the oscillatory structures increase with the increment of SOA length.

C. *FWM pulsewidth*

For weak input pulses regime, the FWHM of the SOA is constant for different SOA lengths and it is 5.6 ps. But, for strong input pulse regime, the FWHM of the FWM pulse increases when the length of the SOA increases. Fig. 4 shows the dependencies of the FWHM to the length of SOA. As the unsaturated gain of the SOA, G_0 is dependent to the length of the SOA, for longer SOA mediums, the leading edge of the pulse experiences a higher gain. So, the leading edge points of the pulse amplified sooner. But, the trailing edge of the pulses experiences the same gain, because in high power regime, the leading edge of the pulse saturates the SOA. So, the pulsewidth of the generated FWM signal increases with the increasing of the SOA length.

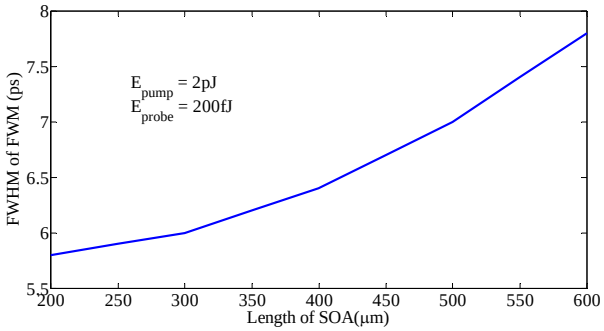

Fig. 4 FWHM of the generated FWM signal for various SOA lengths, for this case, the input pump and probe pulse energies are $2\,pJ$ and $200\,fJ$ respectively.

D. *FWM Signal Peak shift*

For the weak input pulses the peak of the generated FWM signal did not change when the length of the SOA increased. The peak shift is constant at -100 fs.

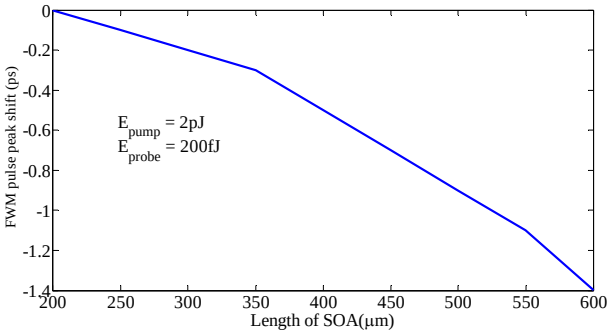

Fig. 5 The generated FWM pulse peak shift for various values of SOA length, for this case, the input pump and probe pulse energies are $2\,pJ$ and $200\,fJ$ respectively.

Fig. 5 shows the peak shift of FWM pulse for various SOA lengths in high power input pulses regime. It can be seen that the peak shift increases with the increment of the SOA length.

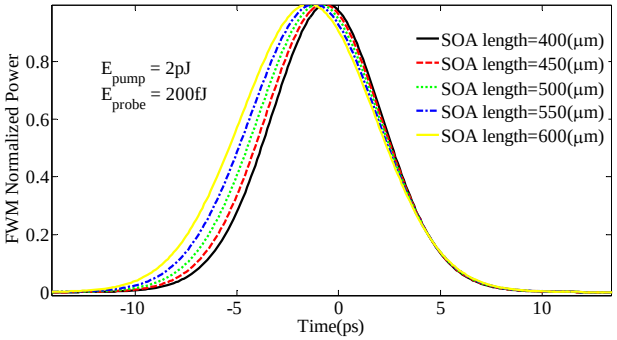

Fig. 6 The normalized shapes of the generated FWM pulse for various values of SOA lengths, for this case, the input pump and probe pulse energies are $2\,pJ$ and $200\,fJ$ respectively.

Fig. 6 shows the normalized FWM signal shapes for various SOA lengths in high power regime. It can be seen that the peak of the FWM pulse has experienced a shift when the length of SOA increased. The pulsewidth of the generated FWM signal is also increases when the SOA length increases. As described before the leading edge of the FWM signal experiences a higher gain for longer SOA mediums.

E. FWM pulse time-bandwidth product

The time-bandwidth product (TBP) of a pulse is the product of its temporal FWHM and spectral width. The TBP product is often used for indicating how close a pulse is to the transform-limited pulse [10].

Fig. 7 shows the variation of FWM pulse's TBP for strong SOA input pulses. When the SOA length increases, the TBP is increases too. But, for weak input pulses regime, the FWM pulse's TBP is constant at 0.385 for different values of the SOA lengths.

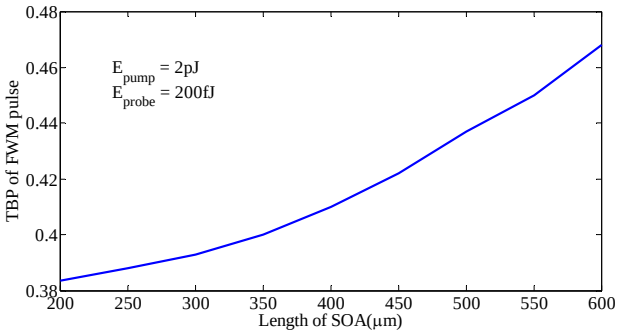

Fig. 7 Time-width product (TBP) of the generated FWM pulse for various values of SOA length, for this case, the input pump and probe pulse energies are $2\,pJ$ and $200\,fJ$ respectively.

As it has shown in Fig 3(b) and Fig.6, both the temporal and spectral width of the generated FWM pulse increased when the SOA length increased. As a result, the TBP increased when the SOA length increased.

F. FWM pulse energy

Fig. 8(a) and Fig. 8(b) show the energy of the FWM pulse for different values of SOA lengths in a weak and strong input pulses regime respectively. SOA length has great influence on the FWM pulse energy. It is come from the relation between unsaturated gain G_0 with the SOA length described in previous section.

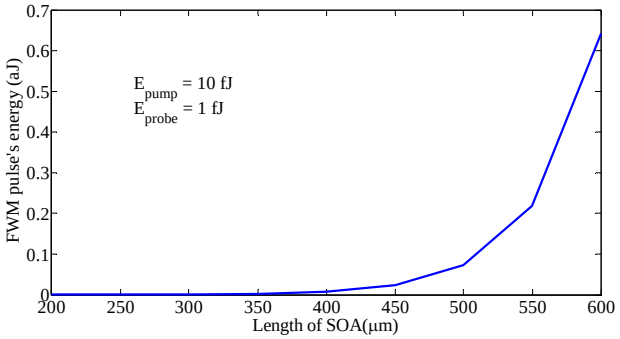

Fig. 8(a) The generated FWM pulse's energy for different SOA lengths, for this case, the input pump and probe pulse energies are $10\,fJ$ and $1\,fJ$ respectively.

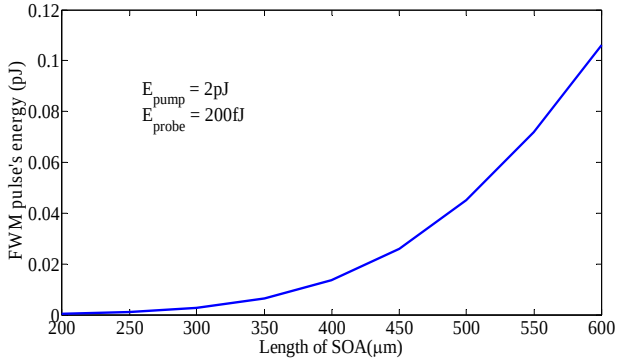

Fig. 8(b) The generated FWM pulse's energy for different values of SOA lengths, for this case, the input pump and probe pulses energies are $2\,pJ$ and $200\,fJ$ respectively.

IV. CONCLUSIONS

In this work, the effects of SOA cavity length has investigated in detail on the FWM signal characteristics for weak and strong SOA input pulses. It has shown that the FWM pulse power increased, when the length of SOA medium increased and for strong input pulses, the FWM pulse shifted when the SOA length increased. For high power input pulses, the FWM signal spectrum has experienced a shift when the medium length increased. Moreover, by increasing the SOA length, the oscillatory structure emerged in FWM spectrum for strong input pulses. It has depicted that FWHM of the FWM pulse is increased, when the cavity length increased for high power regime. Furthermore, the TBP of the pulse is also increasing, when the SOA length increased, but the increment rate is not constant and it depends to the SOA length. In addition, for strong input pulses the peak of the FWM signal has experienced a shift when the length of cavity has changed. The energy of the FWM signal is also dependent to the SOA length and it increases by the increment of the SOA length. Based on our simulation results, we concluded that the FWM signal could be modified by variation of the SOA medium length.

REFERENCES

[1] H. Aghajanpour, V.Ahmadi, M.Razaghi, "Ultra-short optical pulse shaping using semiconductor optical amplifier", *Optics & Laser Technology*, Vol. 41, pp. 654–658, 2009.

[2] E. U. Rafailov, P. Loza-Alvarez, W. Sibbett, G. S. Sokolovskii, D. A. Livshits, A. E. Zhukov, and V. M. Ustinov, "Amplification of Femtosecond Pulses Over by 18 dB in a Quantum-Dot Semiconductor Optical Amplifier", *IEEE Photonics Technology Letters*, Vol. 15, No. 8, pp. 1023-1025, 2003.

[3] M. Razaghi, V. Ahmadi and M. J. Connelly*,"* Comprehensive Finite-Difference Time-Dependent Beam Propagation Model of Counterpropagating Picosecond Pulses in a Semiconductor Optical Amplifier*"IEEE Journal of light wave and technology*, vol. 27, No. 15, pp. 3162-3174, 2009.

[4] M. Razaghi, V. Ahmadi and M. J. Connelly*,"* Femtosecond pulse shaping using counter-propagating pulses in a semiconductor optical amplifier*"*. *Opt Quant Electron*, Springer, 2009.

[5] G. P. Agrawal, N. A. Olsson, "Self-Phase Modulation and Spectral Broadening of Optical Pulses in Semiconductor Laser Amplifiers", *IEEE Journal of Quantum Electronics*, Vol. 25, No.11, PP. 435-442, November. 1989.

[6] Fernandez, P. Morel, and J. W. D. Chi, "Temporal and spectral properties of contra-propagating picosecond optical pulses in SOA," *Opt. Commun.*, vol. 259, no. 2, pp. 465–469, 2006.

[7] N. K. Das, Y. Yamayoshi, and H. Kawaguchi, "Analysis of basic fourwave mixing characteristics in a semiconductor optical amplifier by the finite-difference beam propagation method," *IEEE J. Quantum Electron.*, vol. 36, no. 10, pp. 1184–1192, Oct. 2000.

[8] M. Y. Hong, Y. H. Chang, A. Dienes, J. P. Heritage, P. J. Delfyett, S. Dijaili, and F. G. Peterson, "Femtosecond self- and cross-phase modulation in semiconductor laser amplifiers," *IEEE J. Select. Topics Quantum Electron.*, vol. 2, pp. 523–539, 1996.

[9] S. D. Conte and C. de Boor, "*Elementary Numerical Analysis: An Algorithmic Approach"*, 3rd Ed., Singapore: McGraw-Hill Book Company Co., 1981.

[10] R. Paschotta, "*Encyclopedia of laser physics and technology*", VILEY-VCH, Vol. I, 2008.